Episodic Star Formation Coupled to Reignition of Radio Activity in 3C 236

Tremblay, Grant R.; O'Dea, Christopher P.; Baum, Stefi A.; Koekemoer, Anton M.; Sparks, William B.; de Bruyn, Ger; Schoenmakers, Arno P.

Published in:
The Astrophysical Journal

DOI:
10.1088/0004-637X/715/1/172

Publication date:
2010

The Astrophysical Journal, 715:172–185, 2010 May 20 doi:10.1088/0004-637X/715/1/172

EPISODIC STAR FORMATION COUPLED TO REIGNITION OF RADIO ACTIVITY IN 3C 236

Grant R. Tremblay[1], Christopher P. O'Dea[1], Stefi A. Baum[1], Anton M. Koekemoer[2], William B. Sparks[2], Ger de Bruyn[3], and Arno P. Schoenmakers[3]
[1] Rochester Institute of Technology, One Lomb Memorial Drive, Rochester, NY 14623, USA; grant@astro.rit.edu
[2] Space Telescope Science Institute, 3700 San Martin Drive, Baltimore, MD 21218, USA
[3] Stichting Astronomisch Onderzoek in Nederland, P.O. Box 2, 7990 AA Dwingeloo, The Netherlands
Received 2010 January 25; accepted 2010 April 2; published 2010 April 26

ABSTRACT

We present *Hubble Space Telescope* Advanced Camera for Surveys and STIS FUV/NUV/optical imaging of the radio galaxy 3C 236, whose relic ∼4 Mpc radio jet lobes and inner 2 kpc compact steep spectrum (CSS) radio source are evidence of multiple epochs of active galactic nucleus (AGN) activity. Consistent with previous results, our data confirm the presence of four bright knots of FUV emission in an arc along the edge of the inner circumnuclear dust disk in the galaxy's nucleus, as well as FUV emission cospatial with the nucleus itself. We interpret these to be sites of recent or ongoing star formation. We present photometry of these knots, as well as an estimate for the internal extinction in the source using line ratios from archival ground-based spectroscopy. We estimate the ages of the knots by comparing our extinction-corrected photometry with stellar population synthesis models. We find the four knots cospatial with the dusty disk to be young, of order $\sim 10^7$ yr old. The FUV emission in the nucleus, to which we do not expect scattered light from the AGN to contribute significantly, is likely due to an episode of star formation triggered $\sim 10^9$ yr ago. We argue that the young $\sim 10^7$ yr old knots stem from an episode of star formation that was roughly coeval with the event resulting in reignition of radio activity, creating the CSS source. The $\sim 10^9$ yr old stars in the nucleus may be associated with the previous epoch of radio activity that generated the 4 Mpc relic source, before being cut off by exhaustion or interruption. The ages of the knots, considered in the context of both the disturbed morphology of the nuclear dust and the double–double morphology of the "old" and "young" radio sources, present evidence for an AGN/starburst connection that is possibly episodic in nature. We suggest that the AGN fuel supply was interrupted for $\sim 10^7$ yr due to a minor merger event and has now been restored. The resultant nonsteady flow of gas in the disk is likely responsible for both the new episode of infall-induced star formation and also the multiple epochs of radio activity.

Key words: galaxies: active – galaxies: individual (3C 236) – galaxies: jets – galaxies: starburst

Online-only material: color figures

1. INTRODUCTION

Galaxies occupy a heavily bimodal distribution in color–magnitude space, wherein young, predominantly disk-dominated galaxies reside in a "blue cloud" and evolve onto a characteristically quiescent, bulge-dominated "red sequence" (e.g., Bell et al. 2004; Faber et al. 2007). The underdensity of galaxies in the "green valley" separating these populations implies that cloud-to-sequence evolution is swift, requiring a cessation of star formation more rapid than would be expected in passively evolving systems (e.g., Cowie et al. 1996). Quasar- and radio-mode feedback models have been proposed as mechanisms by which star formation may be truncated by the heating and expulsion of gas (Silk & Rees 1998; Hopkins et al. 2005; Croton et al. 2006; Schawinski et al. 2006), as it is now known that quasar activity was 2 orders of magnitude more common at redshifts $z \sim 2$ than at the present time (e.g., Schmidt et al. 1991). This, considered in the context of declining star formation rates (SFRs) in massive galaxies at $z \sim 2$ (e.g., Pérez-González et al. 2008), along with the emerging consensus that most populations of galaxies harbor quiescent black holes at their centers (hereafter BHs; e.g., Kormendy & Richstone 1995), has given rise to questions of whether all bright galaxies go through one or more active phases (e.g., Haehnelt & Rees 1993; Cavaliere & Padovani 1989). In this scenario, the quenching of star formation via feedback from active galactic nuclei (AGNs) may be one of the primary drivers of cosmic downsizing (e.g., Cowie et al. 1996; Scannapieco et al. 2005, and references therein).

The relationship between the AGN duty cycle and the regulation of host galaxy stellar evolution is far more complicated, however, as it can play competing roles at successive stages of galactic evolution. AGN activity has been associated not only with quenching star formation on large scales, but also triggering it via interstellar medium (ISM) cloud compression from the propagating relativistic jets associated with radio galaxies (e.g., the so-called alignment effect; Rees 1989; Baum & Heckman 1989; McCarthy 1993; Best et al. 2000; Privon et al. 2008). Moreover, it is natural to expect a correlated (but not necessarily causal) relationship between AGN activity and star formation. The tight relationship between BH mass and host galaxy bulge velocity dispersion (Magorrian et al. 1998; Ferrarese & Merritt 2000; Gebhardt et al. 2000) implies that the growth of the BH and the galaxy bulge are tightly coupled (e.g., Kauffmann & Haehnelt 2000; Ciotti & van Albada 2001). It is therefore expected that, throughout the process of hierarchical galaxy formation, gas infall due to major mergers or tidal stripping from a gas-rich companion can fuel not only AGN, but also the growth of the host galaxy stellar component via infall-induced starbursts (e.g., di Matteo et al. 2005). A significant fraction (∼30%) of nearby powerful radio galaxies exhibit evidence of infall-induced starbursts near their nuclei (Smith & Heckman 1989; Allen et al. 2002; Baldi & Capetti 2008; Tremblay et al. 2009), suggesting that the phenomenon is both common and comparable to the lifetime of the radio source ($\sim 10^7$–10^8 yr; e.g., Parma et al. 1999). The AGN/starburst connection is therefore likely real and fundamental to galaxy evolution itself, and its

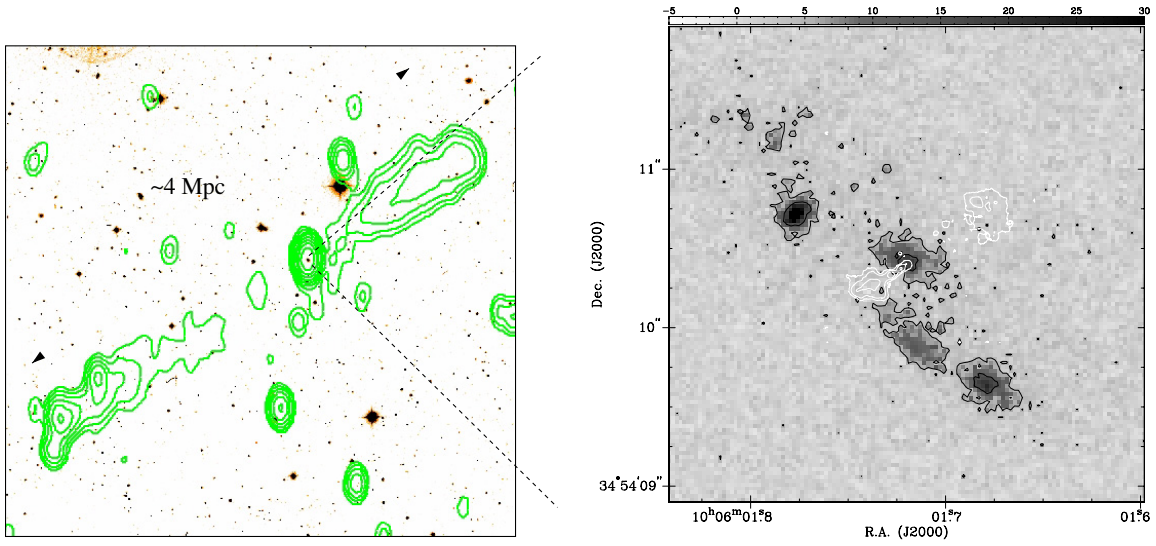

(a) (b)

Figure 1. Two radio sources associated with 3C 236. (a) 326 MHz WSRT radio contours (in green, from Mack et al. 1997) of the "relic" radio emission associated with 3C 236, overlaid on SDSS imaging of the same region of sky. The deprojected size of the jet is ∼4.5 Mpc, making it the second largest known radio galaxy and one of the largest objects in the universe. (b) Global VLBI 1.66 GHz radio contours of the central 2 kpc CSS ("young") radio source from Schilizzi et al. (2001), overlaid on *HST*/STIS NUV imaging of the star-forming knots described by O'Dea et al. (2001). The jet axes of the Mpc- and kpc-scale radio sources are aligned on nearly the same position angle.

(A color version of this figure is available in the online journal.)

characterization has been a major pursuit of the past two decades (e.g., Barnes & Hernquist 1991; Silk & Rees 1998; Fabian 1999; di Matteo et al. 2005; Hopkins et al. 2005; Springel et al. 2005; Silverman et al. 2008; Quillen & Bland-Hawthorn 2008).

A key discriminant in understanding the nature and evolution of the AGN/starburst connection may be found in some radio galaxies whose morphology is clear evidence for multiple epochs of AGN activity. Several such examples have been observed (e.g., 3C 219—Bridle et al. 1986; Clarke et al. 1992, 0108+388—Baum et al. 1990), and have come to constitute a new class of "double–double" radio sources, representing ∼5%–10% of predominantly large (>1 Mpc) radio galaxies (e.g., Schoenmakers et al. 2000a, 2000b). Double–doubles are characterized by outer ("older") and inner ("younger") radio sources propagating outward amidst the relic of the previous epoch of activity. This apparently repetitive activity is thought to be a consequence of the AGN fuel supply having been interrupted, whether by exhaustion, smothering, or disturbance, at some time in the past (Baum et al. 1990). This scenario is consistent with models of radio galaxy propagation (e.g., Kaiser et al. 2000; Brocksopp et al. 2007). The relative ages of the radio sources (and therefore the timescale over which the engine was cut off and reignited) can be estimated using size estimates from radio maps coupled with a dynamical model for the jets and radio spectral energy distributions (SEDs) of the radiating electrons (Schoenmakers et al. 2000a, 2000b; O'Dea et al. 2001).

1.1. An Important Test Case: 3C 236

The nearby ($z = 0.1005$) double–double radio galaxy 3C 236 is an important test case in studies of the AGN/starburst connection, and is the basis of both this paper and a previous study by O'Dea et al. (2001). 3C 236 is a powerful double–double with a relic edge-brightened FR II (Fanaroff & Riley 1974) radio source whose deprojected linear extent exceeds 4 Mpc, making it the second largest known radio galaxy (only J1420−0545 is larger; Machalski et al. 2008), and even one of the largest objects in the universe (Schilizzi et al. 2001). Its inner young compact steep spectrum (CSS) source, whose apparent origin is cospatial with the nucleus, is only 2 kpc in extent and is morphologically reminiscent of a young classical double. Anecdotally, 3C 236 was initially classified as a pure CSS source before it was associated years later with the massive relic FR II source (R. Laing 2009, private communication). The jet propagation axes of both the Mpc- and kpc-scale sources are aligned to within ∼10° of one another (as projected on the sky). See Figure 1 for radio contour overlays of both sources, using 326 MHz Westerbork Synthesis Radio Telescope (WSRT) and 1.66 GHz Global Very Long Baseline Interferometry (VLBI) Network radio mapping from Mack et al. (1997) and Schilizzi et al. (2001) for the relic and CSS sources, respectively.

In addition to its rare radio morphology, 3C 236 is also unique in that its nuclear dust complex is made up of an inner circumnuclear dusty disk that is somewhat misaligned with an apparently separate outer dust lane (Martel et al. 1999; de Koff et al. 2000; Tremblay et al. 2007). The total dust mass in the complex is estimated to be $\sim 10^7\ M_\odot$, based on *Hubble Space Telescope* (*HST*) absorption maps and *IRAS* luminosities (de Koff et al. 2000). In Figure 2, we present a 1.6 μm/0.7 μm absorption map of the dust complex, originally presented in Tremblay et al. (2007) and made via division of *HST*/NICMOS and Wide-Field Planetary Camera 2 (WFPC2) data from Martel et al. (1999) and Madrid et al. (2006), respectively.

The work by O'Dea et al. (2001) studied *HST* NUV and optical imaging of the central few arcsec of 3C 236, finding four knots of blue emission arranged in an arc along the dust lane in the galaxy's nucleus. Their original NUV data are presented in gray scale with black contours in Figure 1(b). The lack of an obvious spatial relationship between the knots and the CSS source suggests that the starbursts are infall induced rather than jet induced. Martel et al. (1999) had also detected the knots of emission in their *HST R*-band imaging, albeit to a lesser degree as the knots are very blue. O'Dea et al. (2001) used

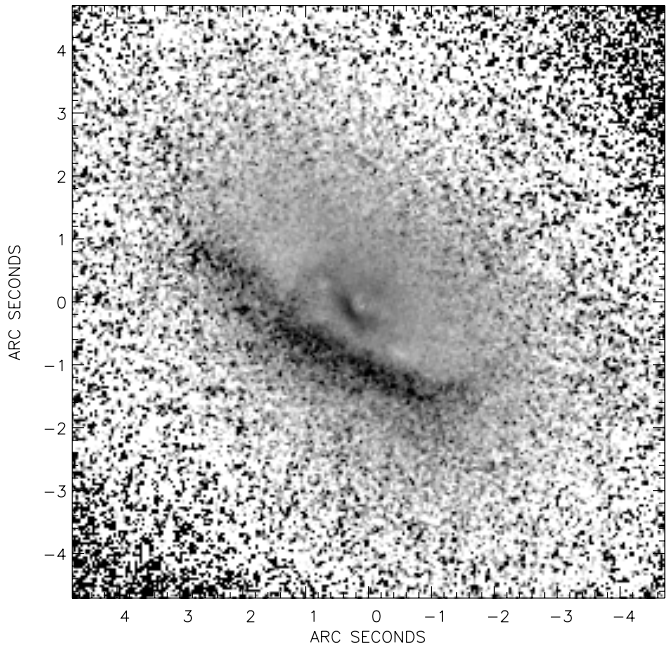

Figure 2. 1.6 μm/0.7 μm colormap of the outer lane and inner dusty disk in the nucleus of 3C 236, made via division of *HST*/NICMOS and WFPC2 data from Martel et al. (1999) and Madrid et al. (2006), respectively. This absorption map was originally presented in Tremblay et al. (2007).

their photometry in comparison with stellar population synthesis models to estimate upper limits to the ages of the individually resolved star-forming knots (seen in Figure 1(b)). They found disparate ages between the clumps of emission, finding two to be relatively young with ages of order $\sim 10^7$ yr, while the other two were estimated at $\sim 10^8$–10^9 yr old, comparable to the estimated age of the giant relic radio source. O'Dea et al. (2001) argued that 3C 236 is an "interrupted" radio galaxy, and has undergone two starburst episodes approximately coeval with the two epochs of radio activity observed on Mpc and kpc scales. That work motivated follow-up observations with *HST* at higher sensitivity and spatial resolution, the results of which we present in this paper.

We organize this work as follows. In Section 2, we describe the new and archival data presented in this paper, as well as the associated data reduction. In Section 3, we present our results, including a comparison of our photometry with stellar population synthesis models, following (in the interests of consistency) the analysis strategy used in O'Dea et al. (2001). We discuss our results in Section 4, focusing on the role played by the AGN/starburst connection in the special test-case environment of 3C 236. We summarize this work and provide some concluding remarks in Section 5. Throughout this paper, we use $H_0 = 71$ km s^{-1} Mpc^{-1}, $\Omega_M = 0.27$, and $\Omega_\Lambda = 0.73$.

2. OBSERVATIONS AND DATA REDUCTION

We present *HST* observations of the nucleus of 3C 236 obtained as part of the Cycle 12 GO program 9897 by O'Dea and collaborators. These consist of *U*- and *V*-band imaging with the Advanced Camera for Surveys (ACS) High Resolution Channel (HRC), FUV imaging with the ACS Solar Blind Channel (SBC), and NUV imaging with the Space Telescope Imaging Spectrograph (STIS). Below we describe the specifics of each new observation presented in this paper, and provide a brief description of the archival imaging and spectroscopy that we also include in our analysis. We also describe the steps taken to reduce the data. A summary of the new and archival *HST* observations utilized in this work can be found in Table 1.

2.1. Cycle 12 ACS and STIS Imaging

Our *HST*/ACS observations were designed to enable high sensitivity multicolor photometry allowing for construction of an SED of the blue knots previously observed in 3C 236 (O'Dea et al. 2001). The FUV, NUV, *U*, and *V* bands were chosen so as to provide multiple constraints on a young blue stellar population, while also enabling consistency checks and estimates on the amount of intrinsic reddening. At the redshift of 3C 236 ($z = 0.1005$), the *U* and *V* bands are located just blueward and redward of the 4000 Å break, respectively. Exposure times were chosen to permit detection of the knots at adequate signal-to-noise ratio (S/N) over a range of possible ages and intrinsic properties. Three orbits (6900 s) were obtained for the SBC FUV image using the F140LP long pass filter. We obtained one orbit each (∼2500 s) for the HRC *U*- and *V*-band images using the F330W and F555W filters, respectively. The F140LP long pass filter on ACS SBC ranges from ∼1350 Å (with a hard cutoff) to ∼2000 Å with a pivot wavelength of 1527 Å. The SBC Multianode Microchannel Array (MAMA) has a spatial resolution of ∼0.″034 × 0.″030 per pixel and a nominal field of view of 34.″6 × 30.″1. The SBC achieves a peak efficiency of 7.5% at 1250 Å. The F330W and F555W filters on ACS HRC have central wavelengths (filter widths) of 3354 (588) Å and 6318 (1442) Å, respectively. The HRC has a pixel scale of 0.″028 × 0.″025 per pixel and its field of view is 29″ × 26″. It reaches a peak efficiency of 29% at ∼6500 Å.

We have also obtained one orbit (2520 s) of NUV imaging with the Cs_2Te MAMA detector on STIS. The F25SRF2 filter has a central wavelength of 2320 Å and an FWHM of 1010 Å, which permits geocoronal [O I]λ1302 + 1306 Å contamination in its bandpass, though its contribution is far lower than the detector background and is not expected to affect our results. The F25SRF2 cutoff does not permit geocoronal Lyα emission. The NUV-MAMA has a pixel scale of 0.″024 and a field of view of 25″ × 25″.

2.2. Archival Data

In this paper, we make use of archival *HST* WFPC2 imaging in *V* and *R* bands (F555W and F702W filters, respectively) obtained as part of the 3CR snapshot programs by Sparks and collaborators (de Koff et al. 1996; McCarthy et al. 1997; Martel et al. 1999). We also use the 1440 s STIS NUV-MAMA F25SRF2 image of 3C 236, which formed the basis of the study by O'Dea et al. (2001), and was formally presented as part of a data paper by Allen et al. (2002). The *H*-band image obtained with the *HST* Near-Infrared Camera and Multiobject Spectrograph (NICMOS2) in SNAP program 10173 (PI: Sparks; Madrid et al. 2006; Tremblay et al. 2007; Floyd et al. 2008) was used for fits to the host galaxy isophotes. Imaging and spectroscopy from the Sloan Digital Sky Survey (SDSS) is also used (York et al. 2000; Adelman-McCarthy et al. 2008).

2.3. Data Reduction

The previously unpublished *HST* data presented in this paper were reduced using the standard On-the-Fly Recalibration (OTFR) pipeline provided as part of the Multi-mission Archive at Space Telescope (MAST). For ACS, the OTFR pipeline combines calibrated and flat-fielded dithered exposures using

Table 1
Summary of Observations of 3C 236

Observatory (1)	Instrument (2)	Aperture (3)	Filter/Config. (4)	Waveband/Type (5)	Exp. Time [Orbits] (6)	Reference (7)	Obs. Date (8)	Comment (9)
New observations								
HST	ACS	HRC	F330W	*U*-band imaging	2516 s [1]	*HST* 9897	2003 Oct 21	SF knots
HST	ACS	HRC	F555W	*V*-band imaging	2612 s [1]	*HST* 9897	2003 Oct 22	Dust lanes
HST	ACS	SBC	F140LP	FUV imaging	6900 s [3]	*HST* 9897	2003 Oct 21	SF knots
HST	STIS	NUV-MAMA	F25SRF2	NUV imaging	2520 s [1]	*HST* 9897	2003 Oct 19	SF knots
Archival observations								
HST	WFPC2	PC1	F702W	*R*-band imaging	4 × 140 s	*HST* 5476	1995 May 7	Galaxy
HST	WFPC2	PC1	F555W	*V*-band imaging	2 × 300 s	*HST* 6384	1996 Jun 12	Galaxy & Dust
HST	STIS	NUV-MAMA	F25SRF2	NUV imaging	1440 s	*HST* 8275	1999 Jan 3	SF knots
HST	NICMOS	NIC2-FIX	F160W	NIR imaging	1152 s	*HST* 10173	2004 Nov 2	Host isophotes

Notes. A summary of the new and archival observations used in our analysis. (1) Facility name; (2) instrument used for observation; (3) configuration of instrument used; (4) filter used; (5) corresponding waveband and specification of whether the observation was imaging or spectroscopy; (6) exposure time (if the observatory is *HST*, the corresponding number of orbits also appears in brackets); (7) corresponding reference for observation. If the observatory is *HST*, the STScI-assigned program number is listed; (8) date of observation; (9) comment specific to observation.

the `multidrizzle` routine with the default parameters. The task calculates and subtracts a background sky value for each exposure, searches for additional bad pixels not already flagged in the data quality array, and drizzles the input exposures into outputs that are shifted and registered with respect to one another. From these drizzled exposures, a median image is created, which is then compared with original input images so as to reject cosmic rays on the drizzled median. More information on the specifics of `multidrizzle` can be found in Koekemoer et al. (2002).

We have not performed post-pipeline processing on the two one-orbit ACS HRC drizzled images (*U* and *V* bands), as for the purposes of this work we are concerned primarily with high surface brightness emission near the center of the galaxy, and the results from the OTFR pipeline were sufficiently free of cosmic rays and hot pixels to be deemed "science ready." For the three-orbit ACS SBC data, we combined the three individual calibrated and flat-fielded files manually using `multidrizzle` with the default parameters. The single 6900 s output image was left unrotated with respect to north so as to avoid associated pixel interpolation errors in our photometry. Information regarding the reduction of the archival data utilized in this paper can be found in the appropriate references cited in Section 2.2.

3. RESULTS

In Figure 3, we present the ACS/HRC *V*-band (at left in red) and ACS/SBC FUV (at right in blue) images in panels (a) and (b), respectively. The two images are aligned and on the same scale, with east left and north up. At the redshift of 3C 236, 1″ corresponds to ∼1.8 kpc. In Figure 4(a), we present the same data in Figure 3 as an overlay, with the FUV contours rendered in black on the *V*-band image for a clearer sense of the spatial relationship between the blue star-forming knots (seen in the FUV) and the dust complex (seen in *V* band). We have labeled each blue knot following the scheme in O'Dea et al. (2001) to allow for easier comparison of results. In the original STIS NUV image discussed in O'Dea et al. (2001; see Figure 1(a)), knots "3" and "4" appeared to be separate, individually resolved regions of emission. In our new higher sensitivity and spatial resolution imaging with ACS, we detect these two regions as one filament of emission that extends ∼1″. In the interests of consistency, we have nonetheless named this region with the two labels "3" and "4" originally assigned in O'Dea et al. (2001), and will hereafter refer to the filament as "knot 3 + 4" when discussing both regions as a whole. As in O'Dea et al. (2001), we will also refer to the "nuclear" FUV emission, seen in Figure 4 as the contour cospatial with the nucleus in the underlying *V* band. In Figure 4(b), we overplot the STIS S25SRF2 NUV contours on the same *V*-band image (with colors inverted to highlight the continuum deficit due to the outer dust lane). The blue emission is morphologically nearly identical in both the FUV and NUV, although the higher sensitivity (and longer exposure time) of the ACS data is evident in the FUV contours of Figure 4(a), which map lower surface brightness features than are seen in Figure 4(b). We utilize the ACS/HRC *U*-band image in our analysis, though do not present the image in a figure as it appears nearly identical to the knots in Figures 3(b) and 4.

We present an analysis of these new data in the subsections below, framed in the context of past results from O'Dea et al. (2001).

3.1. The Outer Lane and Inner Dusty Disk

In Figure 3(a), a significant deficit of galaxy continuum due to a dust lane extends ∼10 kpc and runs in a northeast-to-southwest direction south of the nucleus at a position angle (P.A.) of ∼50°. A steep brightness and color gradient defines a ridge north of the outer lane, giving way to an inner circumnuclear disk of gas and dust whose major axis is oriented ∼30° (offset ∼20° from the outer lane). It is not apparent whether the lane and disk are disjoint structures or a continuous, warped distribution of gas and dust. de Koff et al. (2000) estimated the mass of dust in the complex to be $\sim 10^7\ M_\odot$, corresponding to a gas mass $\sim 10^9\ M_\odot$ given the standard gas-to-dust ratio from the literature (Sodroski et al. 1994).

3.2. Properties of the Star-forming Knots

We have measured the total flux from each knot of star formation in the SBC FUV image (Figure 3(b)) as well as the STIS NUV (Figure 4(b)) and HRC *U*-band images. We have also measured the HRC *V*-band flux for knots 2, 4, and the blue emission associated with the nucleus. We have not performed *V*-band photometry for knots 1 and 3 as they are not clearly detected in this band (see Figure 3(a)). Fluxes were measured from the drizzled images using the `apphot` package in IRAF. The default drizzled pixel units for ACS are in electrons s^{-1}, which scales to counts by a factor of the gain. As this is

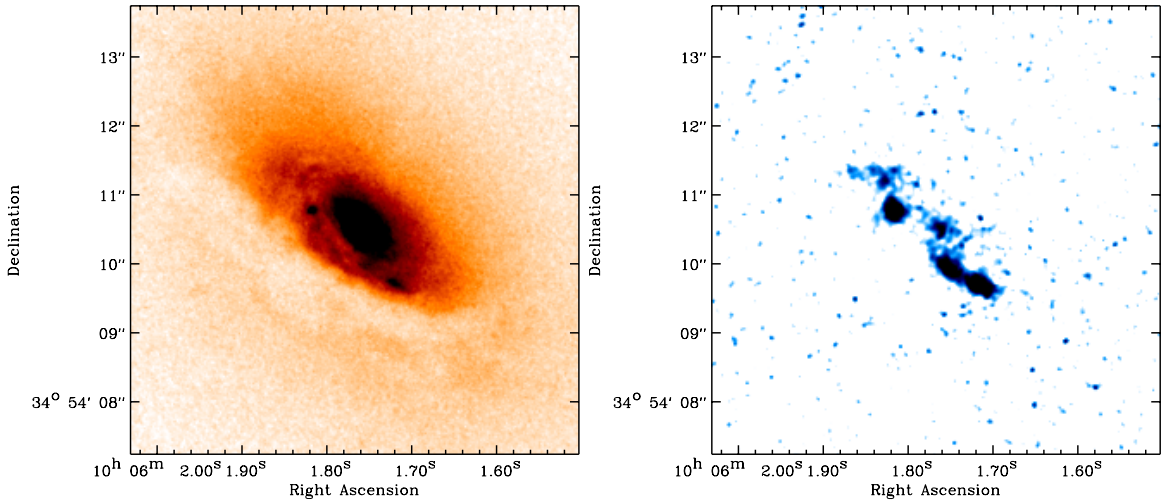

Figure 3. Left: 2500 s *V*-band exposure of the nucleus of 3C 236, using *HST*/ACS HRC with the broadband F555W filter. The outer dust lane is seen in white, while three of the four knots of star formation are seen to the south and west of the nucleus along the inner dusty disk, whose position angle is slightly offset from that of the outer. Right: combined 6900 s *HST*/ACS SBC FUV (F140LP) image of the star-forming knots observed along the inner dust structure of 3C 236. The image has been smoothed with a 2 pixel Gaussian kernel. North is up, east is left. The two images are on the same scale. At a redshift of $z \sim 0.1$, 1″ corresponds to ∼1.8 kpc.

(A color version of this figure is available in the online journal.)

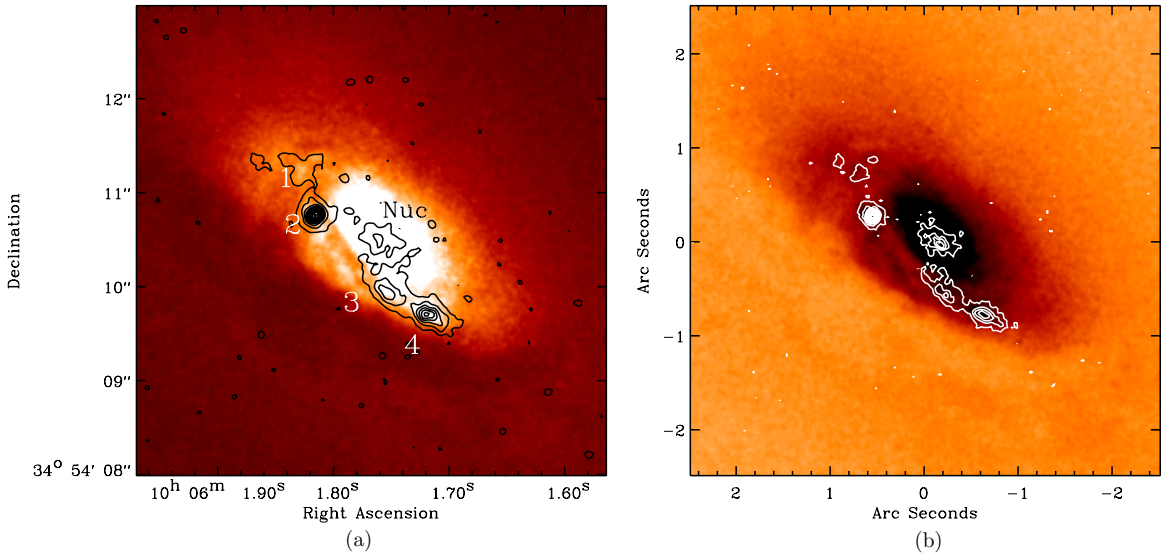

Figure 4. (a) ACS HRC *V*-band image of the nucleus of 3C 236 with ACS SBC FUV contours (smoothed with a 2 pixel Gaussian). The knots of star formation along the inner dust structure have been labeled so as to be consistent with O'Dea et al. (2001). That work detected knots "3" and "4" as two distinct compact regions of emission in their STIS MAMA NUV imaging, while we detect one continuous filament of emission in our more sensitive and higher spatial resolution FUV imaging. So as to maintain consistency with O'Dea et al. (2001) while making this clear we refer to this patch as "knot 3 + 4" throughout this paper. (b) The same HRC *V*-band image (with colors inverted to better emphasize the outer dust lane) with STIS S25SRF2 NUV contours. The knots of star formation are nearly morphologically identical in both the FUV and NUV, though the higher sensitivity of ACS is evident in the FUV contours at left, which highlight lower surface brightness features in the knots. Both panels are aligned and on the same scale. East is left, north is up. At the distance of 3C 236, 1″ corresponds to 1.8 kpc.

(A color version of this figure is available in the online journal.)

corrected for in the pipeline's calibration stage, "counts" and "electrons" can be considered equivalent for the purposes of this paper, regardless of the instrument being discussed. Count rates were summed in an aperture whose radius was chosen based on the size of the source being measured. Background count rates measured through an aperture of the same radius were subtracted from the sum. Photometric conversion into flux units was applied by scaling the residual (source minus background) value by the inverse sensitivity (the PHOTFLAM keyword), converting the value from electrons s^{-1} to flux units in erg cm^{-2} s^{-1} $Å^{-1}$. Statistical 1σ uncertainties were calculated from the measured count rates. The absolute photometric calibration of the ACS SBC, ACS HRC, and STIS MAMA is 5%, 2%, and 5%, respectively.[4] Our photometry was corrected for galactic extinction using the scaling relation by Cardelli et al. (1989) and a color excess $E(B-V) = 0.011$, as listed in the NASA/IPAC Extragalactic Database (NED). Summed and galactic extinction-corrected counts were also converted to magnitudes normalized to the *HST* VEGAMAG system, defined such that the magnitude of Vega is zero in all *HST* bandpasses.

As estimate on the *intrinsic* color of each knot is required in our analysis, and as each star-forming knot is likely embedded in a great deal of dust, we have also corrected all photometry for estimated internal extinction. We had originally proposed for

[4] Maybhate et al. (2010).

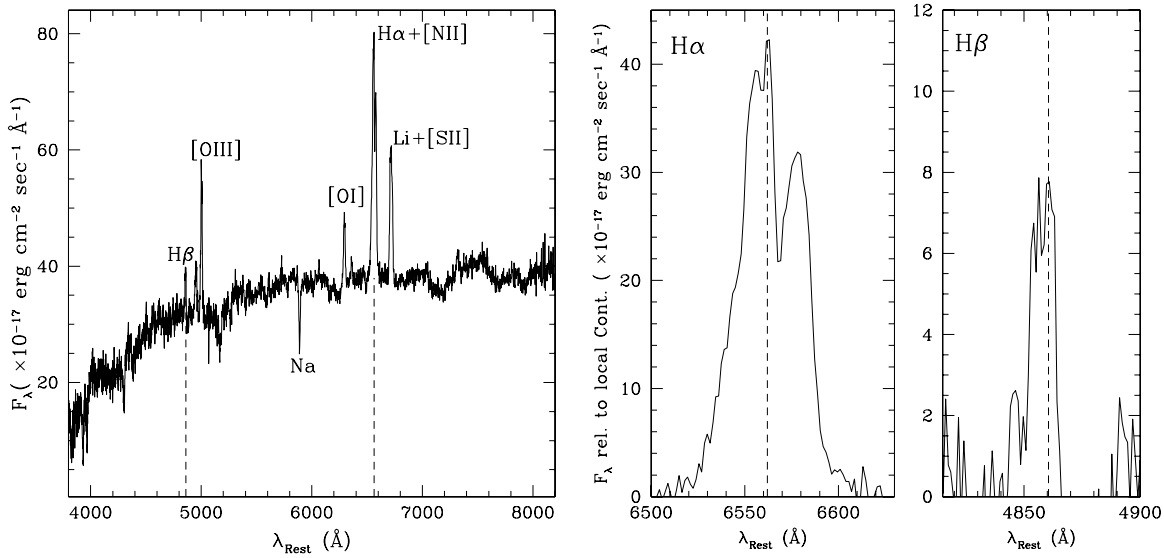

Figure 5. Left: Sloan Digital Sky Survey (SDSS) spectroscopy of the host galaxy of 3C 236. Significant emission and absorption lines have been labeled, and the positions of Hα and Hβ, the lines most relevant for our purposes, have been marked with vertical dashed lines. The spectrum has been shifted to the rest frame using the known redshift of 3C 236 at $z = 0.1$. Right: "zoom in" of the Hα and Hβ lines from the spectrum normalized to their local continuum. SDSS data are of sufficient spectral resolution to resolve the two [N II] lines at 6548 Å and 6583 Å about Hα at 6563 Å (marked with a vertical dashed line). Buttiglione et al. (2009) measured the Balmer decrement $F_{H\alpha}/F_{H\beta} = 4.54$. See Table 4 for other emission line measurements.

and received STIS low dispersion long-slit spectroscopy to allow measurement of the Balmer decrement (Hα/Hβ flux ratio) in a 2″ slit aligned with the knots, however, a pointing error rendered the data unusable. In lieu of this, we use the measured Balmer decrement from Buttiglione et al. (2009), who presented line fluxes for 3C 236 using available SDSS spectroscopy.

Assuming an intrinsic Hα/Hβ theoretical line ratio of 2.86 (i.e., a "case B" recombination scenario is assumed; Osterbrock & Ferland 2006), the observed Balmer decrement allows us to estimate the color excess associated with the internal extinction in the source, following the parameterization of Cardelli et al. (1989) as described in Atek et al. (2008):

$$E\,(B-V)_{\mathrm{H}\alpha/\mathrm{H}\beta} = \frac{2.5 \times \log\,(2.86/R_{\mathrm{obs}})}{k\,(\lambda_\alpha) - k\,(\lambda_\beta)}, \qquad (1)$$

where $R_{\mathrm{obs}} = F\,(\mathrm{H}\alpha)\,/F\,(\mathrm{H}\beta)$ is the observed flux ratio, and the extinction curves at Hα and Hβ wavelengths are $k\,(\lambda_\alpha) \approx 2.63$ and $k(\lambda_\beta) \approx 3.71$, respectively, as given by Cardelli et al. (1989). The Balmer decrement for 3C 236 measured by Buttiglione et al. (2009) of $R_{\mathrm{obs}} \approx 4.54$ yields an $E\,(B-V)_{\mathrm{H}\alpha/\mathrm{H}\beta} \approx 0.465$. The spatial resolution of the SDSS spectroscopy, while lower than that of *HST*, nonetheless allows for a reasonably believable estimate of the internal extinction in the nucleus. In Figure 5, we present the SDSS data for 3C 236, with a "zoom in" on the Hα and Hβ lines in Figure 5(b). As for the purposes of this paper, we are primarily interested in the spectroscopy solely for the Balmer decrement, we do not fit any of the lines and instead use only the analysis from Buttiglione et al. (2009). We do note that a narrow Hα absorption feature appears to be superimposed over the Hα+[N II] lines, and possibly offset from the peak in the emission in velocity space. Hα absorption has been associated with hot stars (Robinson et al. 1990), though we cannot confidently associate the feature with anything specific in the nucleus, as the spectrum is spatially blended over that size scale.

Moreover, the lower spatial resolution of SDSS prohibits us from quantifying how patchy the extinction may or may not be on size scales of a few kpc (of order the scale over which the knots are distributed). It is not unreasonable to think that one knot may be more deeply embedded in the dust disk (and thus more significantly reddened) than another. Regardless, we expect that any variation in reddening between knots due to unresolved patchy extinction will be reasonably small when compared to the overall intrinsic reddening in the nucleus. Were this not the case, we would expect to see more severe color gradient shifts in the absorption map presented in Figure 2. Instead, the colors of the outer lane and inner disk appear to be quite uniform over their projected lengths.

In Table 2, we present the results from our photometric analysis, including measured FUV flux, magnitudes, and colors for each knot. The data are presented first with only galactic extinction corrections applied, and then again with both galactic and internal extinction corrections applied. These corrections are given in Table 3. As the colors are always computed in magnitudes as "shorter wavelength" − "longer wavelength," larger (more positive) values correspond to redder knots. As in O'Dea et al. (2001), we find that the knots vary relatively significantly in comparing colors that have *not* been corrected for internal extinction (Columns 6–8 in the upper half of Table 2). We note that knots 1 and 3 are significantly redder than 2 and 4. In correcting the colors using our estimate for internal extinction, however, we find that all knots are intrinsically very blue, as expected. The sole exception is the UV-bright emission that is cospatial with the nucleus, which lies significantly redward of the "dust disk knots" in color space, even after the internal extinction correction has been applied. This could be due to an older stellar population or patchy extinction leading to higher reddening along the line of sight toward the nuclear UV emission (or both).

Again, we are unable to quantify whether or not there may be patchy extinction on scales finer than the SDSS spatial resolution. As there is vastly more dust in the nucleus than in regions of the galaxy a few kpc outward from the dust complex (determined from our colormap in Figure 2), we find it likely that we have systematically undercorrected for internal extinction. However, a knot that is more heavily extincted than we have corrected for will be intrinsically bluer and therefore younger.

Table 2
Photometry of the Blue Knots in 3C 236

Source	FUV Flux (erg s^{-1} cm^{-2})	$m_{\rm F140LP}$ (FUV) (mag)	$m_{\rm FS25SRF2}$ (NUV) (mag)	$m_{\rm F330W}$ (U Band) (mag)	$m_{\rm FUV} - m_{\rm NUV}$	$m_{\rm FUV} - m_U$ Band	$m_{\rm NUV} - m_U$ Band
(1)	(2)	(3)	(4)	(5)	(6)	(7)	(8)
Corrected for galactic extinction							
Knot 1	8.305×10^{-18}	22.204 ± 0.025	22.165 ± 0.023	22.074 ± 0.015	0.039 ± 0.034	0.130 ± 0.029	0.091 ± 0.027
Knot 2	1.771×10^{-17}	21.382 ± 0.017	21.840 ± 0.019	21.731 ± 0.013	−0.459 ± 0.025	−0.349 ± 0.021	0.109 ± 0.023
Knot 3	1.134×10^{-17}	21.866 ± 0.021	21.865 ± 0.020	21.498 ± 0.012	0.001 ± 0.029	0.368 ± 0.024	0.367 ± 0.023
Knot 4	1.670×10^{-17}	21.427 ± 0.017	21.788 ± 0.019	21.813 ± 0.013	−0.361 ± 0.025	−0.386 ± 0.021	−0.025 ± 0.023
Knot 3 + 4	2.836×10^{-17}	20.871 ± 0.013	20.961 ± 0.013	20.835 ± 0.009	−0.090 ± 0.018	0.036 ± 0.0158	0.126 ± 0.016
Nucleus	9.207×10^{-18}	22.092 ± 0.024	21.613 ± 0.017	20.359 ± 0.007	0.480 ± 0.029	1.733 ± 0.025	1.254 ± 0.018
All	9.037×10^{-17}	19.612 ± 0.008	19.703 ± 0.007	19.125 ± 0.004	−0.091 ± 0.010	0.487 ± 0.008	0.579 ± 0.008
Corrected for galactic and internal extinction							
Knot 1	4.240×10^{-16}	17.934 ± 0.025	18.141 ± 0.023	19.711 ± 0.015	−0.207 ± 0.034	−1.777 ± 0.029	−1.570 ± 0.027
Knot 2	9.044×10^{-16}	17.112 ± 0.017	17.817 ± 0.019	19.369 ± 0.013	−0.705 ± 0.025	−2.258 ± 0.021	−1.552 ± 0.023
Knot 3	5.790×10^{-16}	17.596 ± 0.021	17.841 ± 0.020	19.136 ± 0.012	−0.246 ± 0.029	−1.540 ± 0.024	−1.294 ± 0.023
Knot 4	8.674×10^{-16}	17.157 ± 0.017	17.764 ± 0.019	19.451 ± 0.013	−0.607 ± 0.025	−2.294 ± 0.021	−1.687 ± 0.023
Knot 3 + 4	1.448×10^{-16}	16.601 ± 0.013	16.937 ± 0.013	18.473 ± 0.009	−0.336 ± 0.018	−1.872 ± 0.0158	−1.535 ± 0.016
Nucleus	4.701×10^{-16}	17.822 ± 0.024	17.589 ± 0.017	17.997 ± 0.007	0.232 ± 0.029	−0.175 ± 0.025	−0.407 ± 0.018
All	4.614×10^{-15}	15.342 ± 0.008	15.680 ± 0.007	16.762 ± 0.004	−0.337 ± 0.010	−1.420 ± 0.008	−1.082 ± 0.008

Notes. Photometry of the blue star-forming regions in 3C 236. We have presented our results corrected only for galactic extinction, and then again with galactic and internal extinction corrections applied. The internal extinction correction was estimated from the Balmer decrement using SDSS spectroscopy (see Section 3 and Table 5). 1σ uncertainties have been derived from count rate statistics. The table does not include the systematic errors due to the absolute photometric calibration of the instruments, which are 5%, 2%, and 5% for the ACS SBC (FUV), ACS HRC (U band), and STIS MAMA (NUV), respectively. (1) Source name; (2) measured FUV flux of each blue source from the ACS SBC F140LP image; (3) apparent brightness of the FUV emission in the *HST* VEGAMAG system; (4) apparent brightness in the NUV; (5) apparent brightness in the U band; (6) FUV–NUV color; (7) FUV–U-band color; (8) NUV–U-band color. Larger (more positive) color values correspond to redder colors.

Table 3
Extinction Corrections

Band	Galactic Extinction $A(\lambda)_{\rm Gal}$ (mag)	Internal Extinction $A(\lambda)_{\rm H\alpha/H\beta}$ (mag)
FUV (F140LP)	0.1011	4.270
NUV (F25SRF2)	0.0953	4.025
U band (F330W)	0.0559	2.362
V band (F555W)	0.0292	1.232

Notes. Estimated and calculated corrections to photometry due to galactic and internal extinction. Galactic extinction estimated using $E(B-V) = 0.011$ and the law by Cardelli et al. (1989). Internal extinction calculated from the Balmer decrement $F(\rm H\alpha)/F(\rm H\beta)$ as measured by Buttiglione et al. (2009) from SDSS spectroscopy, using the method described in Osterbrock & Ferland (2006) and in Section 3.3.

Uncertainty therefore lies far more on the "young end" of age estimates than it does on the old, and we are able to estimate upper limits to the ages of the knots as done in O'Dea et al. (2001). We describe these results in the section below.

3.3. Comparison of Photometry with Stellar Population Models

We have compared our photometry with evolutionary models from the stellar population synthesis code STARBURST99[5] (Leitherer et al. 1999; Vázquez & Leitherer 2005). The package incorporates Geneva evolutionary tracks as well as Padova asymptotic giant branch stellar models, and is now widely used for its effectiveness in accounting for all stellar phases contributing to the SED of a young stellar population from the FUV to the NIR. Several simulations were run, with parametric variations in stellar initial mass function (IMF), heavy element abundance, mass range, and whether or not the starburst continuously formed stars at an SFR, or whether it was instantaneous (wherein the starburst is modeled by a delta function, and the resulting population is allowed to age through time).

Simulation results were K-corrected to the redshift of 3C 236 using its luminosity distance of ∼457 Mpc. The corrected model spectra were then convolved through the relevant *HST* filter transmission curve using the photometric synthesis code SYNPHOT[6] in the STSDAS IRAF package. These corrected and convolved models could then be directly compared with our extinction-corrected photometry.

An inherent challenge in comparing our data to predictive population synthesis models lies in the fact that we cannot know for certain what the absolute intrinsic color of each star-forming knot is. As our internal extinction correction is based solely on the Balmer decrement as measured from (relatively) low spatial resolution SDSS spectroscopy, we are able to at best make a rough correction for internal reddening. As such, running several simulations with slight variations in model parameters was largely an exploratory exercise in which we qualitatively characterized how much a model might shift in color–color space given slight changes in, for example, the IMF or heavy element abundance. In general, these variations were found to be small enough such that our uncertain photometry would be unable to discriminate between subtly different models.

Ultimately, however, we are most interested in the rough ages of the knots as this study focuses on a possible coeval relationship between the blue star-forming regions and the reignition of radio activity in the central engine. Model variations are such that our order-of-magnitude age estimates are largely independent of slight changes in model parameters. Moreover, slight variations in our estimate for the internal extinction would not

[5] http://www.stsci.edu/science/starburst99/

[6] http://www.stsci.edu/hst/HST_overview/documents/synphot/

Table 4
Emission Line Ratios and Radio Measurements

Measurement (1)	Value (2)	In Passband ? (3)	Reference (4)
Measured intensities			
log L(Hα)	41.13	No	1
Hβ/Hα	0.22(4)	F555W	1
[O III]λ5007/Hα	0.57(2)	F555W	1
[O I]λ6364/Hα	0.30(3)	No	1
[N II]λ6584/Hα	0.69(1)	No	1
[S II]λ6716/Hα	0.49(2)	No	1
[S II]λ6731/Hα	0.35(3)	No	1
log L(178 MHz)	33.56	N/A	2
log L(5 GHz)	31.62	N/A	3
Estimated UV line intensities			
Lyα/Hα	~6.7	No	
C IV λ1549/Hα	~1.2	F140LP, NUV-MAMA	4
He II λ1549/Hα	~0.3	F140LP, NUV-MAMA	4
N III]λ1750/Hα	~0.1	F140LP, NUV-MAMA	4
C III]λ1909/Hα	~0.3	NUV-MAMA	4
Mg II λ2798/Hα	~0.1	F330W	4

Notes. (1) De-reddened logarithm of luminosity in erg s^{-1} or line ratio (with respect to Hα); (2) measured value, with errors parenthetically presented as percentages; (3) remark if the line (at the redshift of 3C 236) falls into one of the *HST* passbands used in this study; (4) reference. UV line intensities were estimated using measured ratios from the nucleus of M87. Significant uncertainties are associated with these estimates.

References. (1) Buttiglione et al. 2009; (2) Spinrad et al. 1985; (3) Buttiglione et al. 2010; (4) Dopita et al. 1997.

affect the shape of the observed SED so much that we would associate it with a significantly older or younger starburst. As such, we will focus our discussion on the "best-fit" model we have found, with the caveat that all results presented in this section are uncertain and highly dependent upon the intrinsic SEDs of the knots, which we can only roughly estimate.

It is also important to note that there is line contamination in our broadband filters that we have not corrected for, and it is necessary to quantify how much this might affect our results, particularly for the FUV emission in the nucleus. In Table 4, we list intensities of selected bright emission lines (both directly measured from SDSS spectroscopy as analyzed by Buttiglione et al. 2009, and estimated using line ratios from Dopita et al. 1997, measured in the M87 nucleus). In Column 3 of the table, we remark on whether or not the line falls within a passband used in our observations. Relative to this work, there is significant uncertainty associated with these line fluxes given the mismatch between SDSS resolution and fiber placement and the blue star-forming regions we are interested in. Moreover, there are even greater uncertainties in the estimated UV line strengths (as they are derived from ratios measured for the nucleus of M87, not 3C 236). We therefore use these fluxes only to roughly address the possible impact of line contamination on our results. There are relatively bright lines contaminating our optical and UV passbands, namely, [O III]λ5007 (in ACS HRC F555W) and C IVλ1549 (in ACS SBC F140LP and STIS NUV-MAMA). However, correcting for this contamination would not change the overall shape of the SED relative to the comparison STARBURST99 model (which itself includes stellar and nebular emission, and as mentioned above, has been redshifted and convolved through the appropriate bandpass). Even correcting the photometry by as much as a factor of 2 would not affect the age estimate we would ultimately end up making, both for the knots in the dusty disk as well as for the nuclear FUV

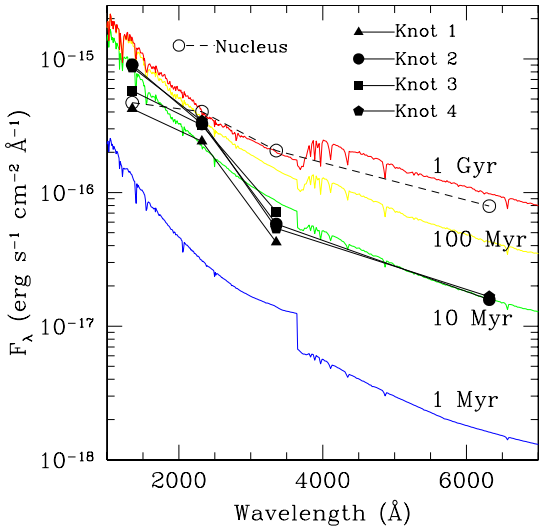

Figure 6. SEDs of the blue star-forming knots as measured in our data, compared with synthetic SEDs as predicted by STARBURST99 stellar population synthesis models. We plot four "snapshot" epochs of one standard STARBURST99 model, normalized to a continuous star formation rate of 1 $M_\odot$ yr^{-1}, a Salpeter IMF of slope $\alpha = 2.35$, upper and lower mass limits of 100 $M_\odot$ and 1 $M_\odot$, respectively, and solar abundances where $Z = 0.020$. Other continuous star formation models were tested, but are not plotted here as variation in overall SED slope and normalization was minimal. In black, we overplot the fluxes of the blue star-forming knots, as well as the red nucleus, using our photometry as corrected for galactic and internal extinction (using the Balmer decrement). Individual knots are identified as per the legend in the upper right corner, using the naming convention for the knots described in Figure 4.

(A color version of this figure is available in the online journal.)

emission. We therefore do not correct our photometry for line contamination, given the uncertainties mentioned above, and because it ultimately does not affect our results.

In Figure 6, we present the main result of this paper, in which we compare the SEDs of the blue star-forming knots as measured in our data with the synthetic SEDs generated by STARBURST99. We plot four "snapshot" epochs of our best-fit model, normalized to a continuous SFR of 1 $M_\odot$ yr^{-1}, a Salpeter (1955) IMF of slope $\alpha = 2.35$, upper and lower mass limits of 100 $M_\odot$ and 1 $M_\odot$, respectively, and solar abundances where $Z = 0.020$. These "snapshot" epochs are 1 Myr (lowest line in blue), 10 Myr (second-to-lowest SED in green), 100 Myr (second highest in yellow), and 1 Gyr (top SED in red). As discussed previously, other star formation models were tested, but are not plotted in Figure 6 as variation in overall SED slope and normalization was minimal.

In black, we overplot the measured SEDs of the blue star-forming knots, as well as the blue emission in the nucleus, using our photometry as corrected for galactic and internal extinction. Individual knots are identified as per the legend in the upper right corner of Figure 6, using the naming convention for the knots outlined in Figure 4(a). The black symbols on each SED mark the central wavelengths of the (from left to right) FUV, NUV, *U*-, and *V*-band *HST* filters, respectively. As mentioned in the previous section, we were only able to obtain *V*-band flux measurements for knots 2, 4, and the blue emission associated with the nucleus (as they were the only regions clearly detected in the *V*-band image).

3.3.1. The Ages of the Blue Knots Cospatial with the Dusty Disk

We find the SEDs of knots 1, 2, 3, and 4 to best match the 10^7 yr model SED. Still, significant variation in color exists among each knot, whose flux in a particular bandpass can vary

by as much as a factor of 5 with respect to the others. Moreover, the SEDs compare somewhat inconsistently with the model (green 10 Myr line in Figure 6), as there is an apparent deficit of emission in the FUV, an excess in the NUV, and another deficit in the *U* band (with respect to the model).

These variations are due to (1) truly intrinsic differences between the colors of the knots, (2) patchy extinction, and/or (3) globally under- or overcorrecting for extinction. While we lack the ability to quantitatively discriminate between these scenarios, we find it naturally likely that a combination of all three work to produce the observed variations. It is also important to note that we are studying UV emission in a very dusty environment that is optically thick to UV photons. The UV emission that we do see is therefore likely emitted on the near side of the clouds with respect to our line of sight, and we know little of the regions of the bursts that are more deeply embedded in the dusty disk. Nevertheless, we can confidently state that the observed SEDs of the knots are more consistent with a 10^7–10^8 yr old starburst than they are with a 10^6 or 10^9 yr old starburst (as modeled by STARBURST99, anyway).

3.3.2. The Age of the UV Emission Cospatial with the Nucleus

Along these lines, we find the nuclear emission to most closely match the 1 Gyr SED, though there is a deficit in its FUV flux with respect to the model (topmost red 1 Gyr line). Assuming that the FUV emission in the nucleus is indeed associated with a 1 Gyr old starburst (an assumption we discuss below), it is possible (and even likely) that this FUV deficit is due to an undercorrection for internal extinction to the nucleus. Such an undercorrection would affect the FUV flux the most, while the *V*-band flux would remain relatively unchanged. The net result would be a steepening of the slope on the blue end, such that the SED of the nucleus might more closely correspond with that of the 1 Gyr model. Moreover, while we cannot quantify how patchy the extinction may be over these scales (as we have discussed several times previously), it is reasonable to imagine the extinction being greater in the nucleus than it is on the edge of the dusty disk, given the inclination of the disk is more edge-on than face-on, such that the nucleus would be farther down the line of sight than the edge of the disk (Tremblay et al. 2007). Regardless, we do not expect that heavier extinction toward the nucleus (in comparison with the knots in the disk) would alter the shape of the nuclear SED so much that it would better correspond with a different age.

Of course, it is important to estimate how much the AGN may contribute to the FUV emission in the nucleus. 3C 236 is a low-excitation radio galaxy (LEG) that lacks broad lines (Buttiglione et al. 2009), suggesting that the accretion region is obscured along our line of sight (i.e., Urry & Padovani 1995). Contribution from the AGN to the nuclear FUV emission would therefore come in the form of scattered light, which we do not expect to contribute significantly to the overall UV excess (certainly not to a degree that would affect our order-of-magnitude age estimates). Holt et al. (2007) similarly fit stellar population models to their ground-based SED for 3C 236, finding that a good fit required a red power-law component, suggestive that the UV excess is not likely associated with scattered light from the AGN and is instead a young, reddened stellar population. Moreover, no point source is visible in any *HST* imaging of the nucleus, and *Spitzer Space Telescope* IR spectroscopy obtained for 3C 236 (Spitzer programs 20719 and 40453 by PI: Baum and collaborators) does not show evidence for a hidden quasar continuum (although formal presentation of these data is forthcoming in future papers). Hence, we expect the majority of the FUV emission in the nucleus to be due to stellar continuum from young stars, whose age we have estimated to be $\sim 10^9$ yr old.

Table 5
Estimated Star Formation Parameters

Source (1)	Est. Required SFR ($M_\odot$ yr^{-1}, Cont. Model) (2)	Est. Required Mass Range (log $M_\odot$, Inst. Model) (3)
Knot 1	0.69	7.3–8.7
Knot 2	1.47	7.7–9.0
Knot 3	0.94	7.5–8.8
Knot 4	1.41	7.7–9.0
Knot 3 + 4	2.36	7.9–9.2
Nucleus	0.47	7.4–8.7
All	7.51	8.4–9.7

Notes. (1) Source identifier; (2) estimated star formation rates (SFRs) using the "best-fit" STARBURST99 "snapshot" epoch as determined based on Figure 6 and as described in Section 4.2. We have chosen the 10^7 yr SED as the "best fit" for all of the knots, and the 10^9 yr SED for the nucleus. The chosen STARBURST99 model for this estimate is normalized to a continuous SFR of 1 $M_\odot$ yr^{-1}, a Salpeter IMF of slope $\alpha = 2.35$, upper and lower mass limits of 100 $M_\odot$ and 1 $M_\odot$, respectively, and solar abundances where $Z = 0.020$. Other models were tested, but those results are not presented here as variation was minimal, and the SFR for each knot is generally of order $\sim$1 $M_\odot$ yr^{-1} regardless of the model. (3) Required mass range of an instantaneous starburst triggered 10^7–10^8 yr ago. The STARBURST99 parameters used are the same as in (2), except the starburst is modeled as a delta function at time zero, rather than forming continuously with an SFR.

3.3.3. The Ages of the Knots in Context of Other Works

To summarize, we conclude from Figure 6 that the four star-forming knots cospatial with the dusty disk are of order $\sim 10^7$ yr old, while the stars in the nucleus are older, with an age of $\sim 10^9$ yr old. In Table 5, we present the SFRs associated with our "best-fit" STARBURST99 continuous star formation model. We also list the mass range required for an instantaneous burst model to reproduce the observed fluxes, while noting that the continuous model is a better match to our data. Nevertheless, the mass ranges we estimate are consistent with those predicted by the instantaneous burst models of O'Dea et al. (2001). Our estimated SFRs are also consistent with those derived from the O'Dea continuous star formation models, and are always on the order of a few $M_\odot$ yr^{-1}. See Table 3 in O'Dea et al. (2001) to compare both their derived SFRs and masses with our results.

Unlike this work, O'Dea et al. (2001) compared their photometry to Bruzual & Charlot stellar population synthesis models (Bruzual A. & Charlot 1993; Charlot & Longhetti 2001) absent an estimate for internal extinction (the required data were not available at the time). They found bimodality in the ages of the knots, wherein knots 1 and 3 were measured to be young, of order $\lesssim 10^7$ yr old, and 2 and 4 were estimated at $\lesssim 10^8$–10^9 yr old. In contrast, we estimate a nearly uniform age distribution among the knots in the dust disk of $\sim 10^7$ yr old, while the FUV emission in the nucleus is likely to be $\sim 10^9$ yr. The difference in results between this work and that of O'Dea et al. (2001) likely arises from (1) different data sets, (2) the lack of internal extinction correction in the O'Dea work (none was available at the time), and (3) comparison with Bruzual & Charlot models versus STARBURST99 models in this work. Whatever the case, the age upper limits we estimate for our knots are consistent with the "young" knots 1 and 3 from O'Dea et al. (2001). That work also clearly emphasizes that the older ages estimated for

knots 2 and 4 are merely upper limits, and entirely dependent upon the intrinsic colors of the knots.

The work by Holt et al. (2007) also estimated the ages of the star-forming regions in 3C 236 by fitting young stellar population models to a ground-based SED from the ESO Very Large Telescope (VLT). Their results are consistent both with O'Dea et al. (2001) and this work, estimating similar ages for the stellar populations. In examining stellar absorption features, they further rule out models with ages $\gtrsim$1.0 Gyr, as those models overpredict the depth of the Ca II feature.

The work by Koekemoer et al. (1999) performed a similar age dating exercise for the centrally dominant radio-loud elliptical galaxy in the cooling flow cluster Abell 2597. Much like 3C 236, that object possesses a compact radio source, a significant filamentary dust lane, and a network of clumpy knots and filaments of blue continuum, which Koekemoer et al. (1999) interpreted to be sites of recent star formation. Using single-burst Bruzual & Charlot models, that work derived ages for the knots of $\sim 10^7$–10^8 yr, comparable to the inferred age of the compact radio source.

4. DISCUSSION

4.1. Dynamics of the Gas and dust in 3C 236

As discussed in Section 3.1 and seen in Figure 3(a), 3C 236 possesses both an outer filamentary dust lane and an inner circumnuclear disk whose semimajor axes are misaligned with one another by $\sim 15^\circ$ (Martel et al. 1999; de Koff et al. 2000; O'Dea et al. 2001). These morphologies are strongly indicative of a galaxy that has recently acquired gas from a companion, suggesting that the outer lane is dynamically young. Below we motivate this assertion using simple dynamical arguments.

Gas and dust acquired through mergers or tidal stripping is expected to coalesce on a dynamical timescale ($\sim 10^8$ yr, e.g.; Gunn 1979; Tubbs 1980) and precess about a symmetry plane of the host galaxy, finally settling into it on a precession timescale of order a Gyr (e.g., Tohline et al. 1982; Habe & Ikeuchi 1985). During this time the gas will dissipate angular momentum and fall inward toward the nucleus at a rate dependent upon the structure of the potential well and the star formation efficiency of the gas (Barnes 1996; Bekki & Shioya 1997). In the scenario proposed by Lauer et al. (2005), filamentary distributions of dust that have not yet reached the nucleus would be classified as lanes, which might be thought of as transient structures that would eventually form a nuclear disk if given sufficient time (e.g., Tremblay et al. 2007, and references therein).

The recent study by Tremblay et al. (2007) lent evidence in support of this scenario. That work described a dichotomy between dusty lanes and disks in a sample of low-redshift ($z < 0.3$) 3CR radio galaxies (including 3C 236), finding round nuclear dusty disks to preferentially reside in round to boxy host galaxies, depending on their inclination with respect to the line of sight. Conversely, filamentary dust lanes which had not yet settled into the nucleus were found to reside exclusively in host galaxies with disky isophotes. Numerical simulations of dissipational mergers have shown that rotationally supported, disky systems are typically the result of gas-rich mergers, while boxy galaxies are often formed through dry (gas-poor) mergers (e.g., Barnes 1996; Bekki & Shioya 1997; Khochfar & Burkert 2005). Past studies of both radio-loud and radio-quiet ellipticals have shown that dust lanes are very often misaligned with the major axis of their host galaxy isophotes, while the opposite is true for dusty disks (e.g., Tran et al. 2001, and references therein). These results support a scenario in which nuclear dusty disks are native to the host galaxy pre-merger, while dust lanes are far younger structures, having recently been externally acquired through tidal stripping or a merger (Tremblay et al. 2007).

3C 236 appears to contain *both* an outer dust lane and inner dusty disk. Moreover, the outer dust lane is slightly misalinged with the major axis of the host galaxy isophotes over a projected 4″ linear extent centered about the nucleus. We mark the isophotal structure of the host in Figure 7(a), in which we have plotted isocontours on 1.6 μm (analog of *H*-band) *HST*/NICMOS imaging from Madrid et al. (2006). In Figure 7(b), we present a "zoomed in" view of the colormap originally presented in Figure 2, with contours marking the misalinged outer lane and inner dusty disk. Note how the dusty disk appears to be better aligned with the major axis of the inner host galaxy isophotes than the lane (Figures 7(a) and (b) are on the same scale). In Figures 7(c) and (d), we plot isophote major axis P.A. and isophotal ellipticity, respectively, as a function of semimajor axis. These data stem from fits to the NICMOS *H*-band isophotes using the IRAF task `ellipse`, originally performed by Donzelli et al. (2007) and analyzed by Tremblay et al. (2007). Note from Figure 7(c) that the isophotes are lopsided, particularly to the southeast between $\sim$2″ and 4″ from the nucleus. The asymmetric isophotes are indicative of a stellar population that has yet to fully relax dynamically, suggesting a recent minor merger has taken place.

Framed in the context of the results discussed above, the dual dust morphologies in 3C 236 present strong evidence of the host galaxy having recently ($\sim 10^9$ yr) acquired gas from a companion. Following the scenario discussed by Tremblay et al. (2007), the inner dusty disk may have been native to the host galaxy *before* the recent gas acquisition event, while the outer lane may be been externally acquired as a result of that event, and is still in the process of migration toward the nucleus.

As dust traces molecular gas accretion reservoirs that fuel AGN activity, this scenario works naturally with the notion that 3C 236 is an "interrupted" radio source. de Koff et al. (2000) estimated the mass of dust in the lane and disk to be $\sim 10^7\ M_\odot$, corresponding to a gas mass of $\sim 10^9\ M_\odot$. Such a significant gas mass could supply fuel to the AGN for a long period of time, allowing the radio galaxy to grow to its very large size (4 Mpc). The relic radio source also lends an unrelated argument in favor of a scenario in which a large fraction of the gas mass was native to the host galaxy *prior* to whatever event cut off or smothered the AGN activity for a period of time (ostensibly the same event responsible for depositing new gas into the system). *Some* significant fuel source was clearly necessary to power such a large radio jet, though it is not clear whether that original source is still present and observed in the form of the inner disk, or whether the original source was exhausted and the dust we observe now traces a newly deposited accretion reservoir. Imagining for a moment that the inner dust disk is old and native to the host "pre-interruption," it is plausible to imagine the inner disk being perturbed, cutting off the BH fuel supply, then resettling back toward the nucleus after a short period of time ($\sim 10^7$ yr), reigniting AGN activity. During this time the young, newly acquired dust from the "interruption" event would begin to settle into a filamentary lane, and begin migration inward toward the nucleus on a much larger timescale (a few times $\sim 10^9$ yr).

The nature of this "interruption" event is not clear. The host galaxy of 3C 236 is in a very poor environment and has no

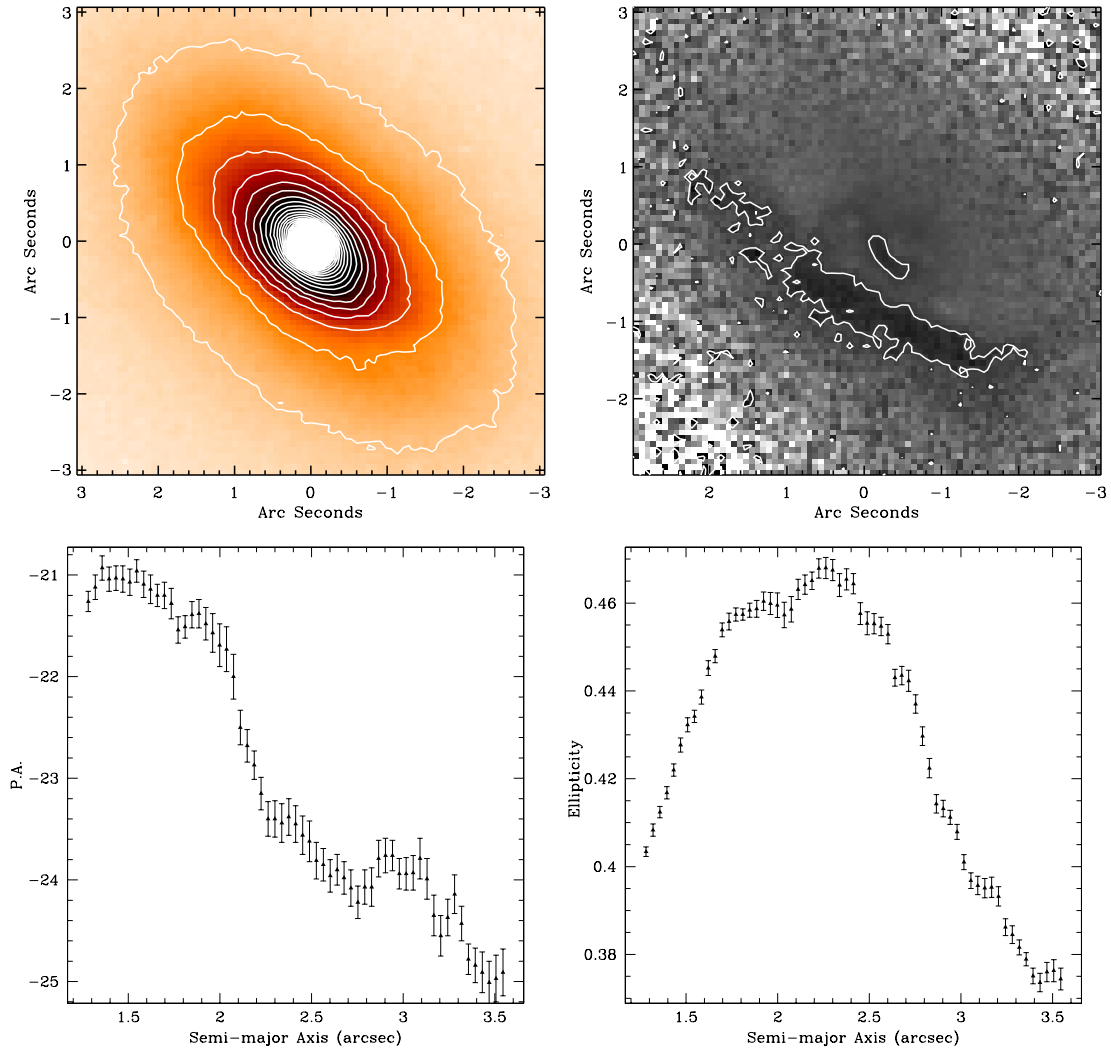

Figure 7. Top left: *HST*/NIC2 1.6 μm image of 3C 236 with highlighted isophotal contours. Top right: 1.6 μm/0.702 μm (H/R-band) colormap of the dusty disk in the nucleus of 3C 236, made via division of *HST*/NIC2 and WFPC2 data. Evidence for two disparate dust structures are seen in the colormap. The position angles (P.A.s) of the outer dust lane and the inner disk-like structure are offset by $\sim$10°. Bottom left: semimajor axis P.A.s of ellipses fit to the *HST*/NIC2 H-band isophotes using the IRAF routine `ellipse`. The plot shows a several sigma twist in the isophotes between 1″ and 3″, which is also visibly evident in the contours of the image at top left. Bottom right: ellipticity of the fit isophotes from `ellipse` over the same scale.

(A color version of this figure is available in the online journal.)

obvious group members within 0.5 Mpc (based on a statistical correction for background contamination; Zirbel 1997). This, combined with the fact that the isophotes of 3C 236, while lopsided, are not highly irregular, suggests that the event was likely a minor merger. In this scenario, the presumably dust-rich and small donor galaxy would have been fully consumed by the much larger 3C 236. Were the event a major merger, one would expect to see more irregularity in the isophotes, as the "dynamically young" dust, the CSS radio source, and the fact that one can still detect the relic radio source even given synchrotron cooling timescales ($\sim 10^8$–10^9 yr) require the merger event to have happened relatively recently (no more than 10^7–10^8 yr ago). A major merger of nearly equal-mass galaxies would likely result in structural irregularities that would last much longer than that timescale.

4.2. Star Formation in the Nucleus in the Context of the Relic Radio Source

Canonical estimates based on synchrotron cooling timescales would suggest that the relic $\sim$4 Mpc FR II radio source is not older than a few times 10^8 yr (e.g., Parma et al. 1999). O'Dea et al. (2001) attempted to better constrain the age of the relic source, arguing that a lower limit to its age $t_{\rm min,relic}$ could be estimated using simple dynamical arguments:

$$t_{\rm min,relic} \simeq 7.8 \times 10^6 \left(\frac{v_{\rm lobe}}{c}\right)^{-1} \ {\rm yr}, \qquad (2)$$

where $v_{\rm lobe}$ is the lobe propagation speed. Using a canonical expansion speed of $\sim 0.03c$ (e.g., Alexander & Leahy 1987), O'Dea et al. (2001) estimated the dynamical age of the relic source to be 2.6×10^8 yr. This would make for an old radio source, near to the time when synchrotron cooling would render the lobes unobservable at higher frequencies as the electrons age. Of course, the relic source associated with 3C 236 is among the largest in the universe, so the fact that it is likely old is not surprising.

If the double–double radio source indeed arises from episodic activity in the AGN, at some stage in the life of 3C 236 its nucleus would have entered a dormant phase and halted the collimation of its jets. This would have deprived the hotspots

of their energy supply on a timescale of order the nucleus-to-hotspot traversal time of the jet material ejected prior to the shut down of the AGN, assuming it advanced relativistically (e.g., Baum et al. 1990; Kaiser et al. 2000; Schoenmakers et al. 2000a, 2000b). The production of "young electrons" in the hotspots by magnetohydrodynamical (MHD) turbulence or Fermi acceleration in the Mach disk is thought to cease when the hotspot is no longer fed by a jet, meaning the electron population will begin to age once the last of the remaining jet material has arrived (e.g., Jones et al. 1999, and references therein). If one believes radio spectral ageing techniques, then the ages of the youngest electrons in the lobe added to the jet traversal time from the nucleus to the hotspot should be of order the timescale over which the nucleus has been dormant. O'Dea et al. (2001) estimated this timescale to be $\sim 10^7$ yr, an order of magnitude younger than the 2.6×10^8 yr dynamical age of the relic source.

Note that the ages estimated by these two techniques need not agree, as the ages of the youngest electrons in the lobe will correspond to the time when jet propagation ceased, but tell us nothing about how long the nucleus may have been active. Moreover, all of these age estimates in the radio are heavily dependent upon assumptions such as the propagation speed and the true source of young electrons. Indeed, the active phase corresponding to the creation of the relic radio source may have been far longer lived than the dynamical age of the relic source itself. We cannot know for certain how much of the lobes may have already cooled past the point of observability. Observations at lower frequencies may be enlightening in this regard.

As discussed in Section 3.3.2, we have estimated the age of the nuclear starburst to be $\sim 10^9$ yr old, given the previously discussed caveats and noting that it may be younger if we have undercorrected for internal extinction to the nucleus. Nevertheless, the approximate ages of the nuclear starburst and the ~4 Mpc relic source are just close enough to warrant noting that they might *possibly* be related to a common gas infall event. Having said that, we again stress that this is only a possibility, and we are unable to draw conclusions relating to such a connection in light of the significant uncertainties involved.

4.3. The Star-forming Knots in the Context of the CSS Radio Source

O'Dea et al. (2001) used arguments similar to those discussed in the above section to estimate the age of the central CSS radio source, operating under the assumption that it was young and not "old and frustrated" (a reasonable assumption, especially in light of recent results on CSS sources, e.g., Holt et al. 2009). Their estimate for its age $t_{\mathrm{min,CSS}}$ was given by

$$t_{\mathrm{min,CSS}} \simeq 3.2 \times 10^3 \left(\frac{v_{\mathrm{lobe}}}{c}\right)^{-1} \ \mathrm{yr}, \qquad (3)$$

where using the same lobe advance speed they found the age of the CSS source to be very young indeed, of order $\sim 1.0 \times 10^5$ yr. As discussed in Section 3.3, we have estimated that the star-forming knots cospatial with the dusty disk are $\sim 10^7$ yr old.

4.4. Is the Recent Episode of Star Formation Coupled to the Rebirth of Radio Activity in 3C 236?

If the recent episode of star formation in the disk were directly related to the event resulting in reignition of radio activity giving birth to the CSS source, we would not necessarily expect a one-to-one correspondence among their ages. The dynamical time on scales of a few kpc, where the star-forming knots are located, is far longer than the dynamical time on sub-pc scales where the AGN is fuelled. In this context, the difference in estimated ages of the star-forming knots and the CSS source would constrain the timescale over which the gas is transported from kpc to sub-kpc scales. This cannot be any longer than the age of the young stars ($\sim 10^7$ yr), which corresponds not only with the dynamical time on kpc scales but also the estimated dormancy period of the nucleus.

The recent work by Wuyts et al. (2009) discusses the merger-driven models of Hopkins et al. (2006) in the context of internal color structure in massive star-forming galaxies. They find internal color gradients to be strongest during the merger phase, with blue star formation expected on scales outside a few kpc (approximately where we observe the star formation in 3C 236). In their previously mentioned work, Koekemoer et al. (1999) derived ages to star-forming knots in Abell 2597 that were closely related to the inferred merger and AGN fuelling timescales giving rise to the compact radio source in that galaxy.

Our observations have yielded similar results, and seem to suggest one possible "story" for the history of 3C 236. In considering its double–double radio morphology in the context of its dynamically young dust complex and recently triggered compact starbursts, we suggest that 3C 236 has undergone multiple epochs of AGN activity due to a nonsteady supply of fuel to the central engine. We suggest that the period of activity related to the 4 Mpc relic source was ended when the fuel supply to the central engine was cut off, whether by exhaustion, strangulation, or disturbance. After a subsequent $\sim 10^7$ yr dormant phase, infalling gas from a minor merger event reached kpc scales, where a starburst was triggered via cloud–cloud collisions amid collapse. The gas not involved in star formation reached the nucleus after a subsequent dynamical time, triggering reignition of the AGN and giving birth to the CSS radio source.

We hesitate to make further suggestions relating to the star formation in the nucleus and its possible connection with the relic source, nor will we suggest whether or not the outer filamentary dust lane and inner disk are two distinct structures with different histories (i.e., recently acquired versus native to the host pre-merger). We have argued in Section 4.1 that discriminating between the two scenarios may shed light on whether the AGN "interruption" event was due to actual *exhaustion* of its fuel supply, or only dynamical *disturbance* of its fuel supply. Whatever the case, the results of this work and those of O'Dea et al. (2001) strongly suggest that the transport of gas to the nucleus of 3C 236 has been significantly nonsteady over the past Gyr, giving rise to a unique galaxy that acts as an important test case in studies of the AGN/starburst connection.

5. SUMMARY AND CONCLUDING REMARKS

We have presented follow-up *HST* ACS and STIS observations of the radio galaxy 3C 236, described by O'Dea et al. (2001) as an "interrupted" radio source. The galaxy is associated with a massive relic ~4 Mpc FR II radio source (making it one of the largest objects in the universe), as well as an inner 2 kpc CSS "young" radio source. This "double–double" radio morphology is evidence for multiple epochs of AGN activity, wherein the BH fuel supply is thought to have been exhausted or cut off at some time in the past, and has only recently been reignited.

We present *HST* FUV, NUV, *U*-, and *V*-band imaging of four star-forming knots, previously described by O'Dea et al. (2001), that are arranged in an arc along the outer edge of the

galaxy's circumnuclear dust disk (which itself is surrounded by a misaligned outer filamentary dust lane). We have also detected blue emission cospatial with the nucleus itself. We describe these observations in detail, as well as the steps taken to reduce the data. We present photometry of the blue knots, and discuss our efforts to correct the data for internal extinction to the source using the Balmer decrement available from archival SDSS spectroscopy.

We compare the measured four-color SEDs of the star-forming knots to synthetic SEDs from STARBURST99 stellar population synthesis models, with the ultimate goal of roughly estimating the ages of the knots. We find that the four knots cospatial with the outer edge of the dusty disk are likely $\sim 10^7$ yr old, while the FUV emission cospatial with the nucleus is likely older, at $\sim 10^9$ yr old (with the caveat that undercorrection for internal extinction in the nucleus would lower this limit). We argue that the ages of the young knots are suggestive of a causal connection with the young central radio source.

We frame these results in the context of 3C 236 as an apparently "interrupted" radio galaxy. Our results are generally consistent with those of O'Dea et al. (2001), and we argue along similar lines that the transport of gas in the nucleus of 3C 236 is nonsteady, wherein the active phase giving rise to the 4 Mpc relic source was cut off by exhaustion or disturbance of the AGN fuel supply. We suggest that this lead to a dormant period punctuated by a minor merger event, and the subsequent infalling gas triggered not only a new episode of star formation, but also ushered the galaxy into a new active phase giving rise to the young CSS radio source.

Results such as these support the natural argument that infalling gas largely fosters the relationship between the growth of the AGN and that of its host galaxy stellar component. In time, that relationship may evolve from mutual growth to the regulation of the latter by the former through quenching from AGN feedback. As infalling gas is a critical component in merger-driven hierarchical models, the triggering of AGN may be fundamental to galaxy evolution itself. In this way, the relevance of 3C 236 might extend beyond studies of episodic activity in radio galaxies to studies of AGN in the context of galaxy evolution as a whole.

We thank Rafaella Morganti, Clive Tadhunter, Alessandro Capetti, and Andy Robinson for helpful discussions. We also thank Ari Laor and the anonymous referee whose helpful comments lead to the improvement of this work. G.R.T. acknowledges B. F. and support from the National Aeronautics and Space Administration (NASA) grant HST-GO-9897, as well as the NASA/NY Space Grant Consortium. This work is based on observations made with the NASA/ESA *Hubble Space Telescope*, obtained at the Space Telescope Science Institute, which is operated by the Association of Universities for Research in Astronomy, Inc., under NASA contract 5-26555. This research has made use of Sloan Digital Sky Survey (SDSS) data products. Funding for the SDSS and SDSS-II was provided by the Alfred P. Sloan Foundation, the Participating Institutions, the National Science Foundation, the U.S. Department of Energy, the National Aeronautics and Space Administration, the Japanese Monbukagakusho, the Max Planck Society, and the Higher Education Funding Council for England. We have also made extensive use of the NASA Astrophysics Data System bibliographic services and the NASA/IPAC Extragalactic Database, operated by the Jet Propulsion Laboratory, California Institute of Technology, under contract with NASA.

REFERENCES

Adelman-McCarthy, J. K., et al. 2008, ApJS, 175, 297
Alexander, P., & Leahy, J. P. 1987, MNRAS, 225, 1
Allen, M. G., et al. 2002, ApJS, 139, 411
Atek, H., Kunth, D., Hayes, M., Östlin, G., & Mas-Hesse, J. M. 2008, A&A, 488, 491
Baldi, R. D., & Capetti, A. 2008, A&A, 489, 989
Barnes, J. 1996, in IAU Symp. 171, New Light on Galaxy Evolution, ed. R. Bender & R. L. Davies (Dordrecht: Kluwer), 191
Barnes, J. E., & Hernquist, L. E. 1991, ApJ, 370, L65
Baum, S. A., & Heckman, T. 1989, ApJ, 336, 681
Baum, S. A., O'Dea, C. P., Murphy, D. W., & de Bruyn, A. G. 1990, A&A, 232, 19
Bekki, K., & Shioya, Y. 1997, ApJ, 478, L17
Bell, E. F., et al. 2004, ApJ, 608, 752
Best, P. N., Röttgering, H. J. A., & Longair, M. S. 2000, MNRAS, 311, 23
Bridle, A. H., Perley, R. A., & Henriksen, R. N. 1986, AJ, 92, 534
Brocksopp, C., Kaiser, C. R., Schoenmakers, A. P., & de Bruyn, A. G. 2007, MNRAS, 382, 1019
Bruzual, A. G., & Charlot, S. 1993, ApJ, 405, 538
Buttiglione, S., Capetti, A., Celotti, A., Axon, D. J., Chiaberge, M., Macchetto, F. D., & Sparks, W. B. 2009, A&A, 495, 1033
Buttiglione, S., Capetti, A., Celotti, A., Axon, D. J., Chiaberge, M., Macchetto, F. D., & Sparks, W. B. 2010, A&A, 509, A6
Cardelli, J. A., Clayton, G. C., & Mathis, J. S. 1989, ApJ, 345, 245
Cavaliere, A., & Padovani, P. 1989, ApJ, 340, L5
Charlot, S., & Longhetti, M. 2001, MNRAS, 323, 887
Ciotti, L., & van Albada, T. S. 2001, ApJ, 552, L13
Clarke, D. A., Bridle, A. H., Burns, J. O., Perley, R. A., & Norman, M. L. 1992, ApJ, 385, 173
Cowie, L. L., Songaila, A., Hu, E. M., & Cohen, J. G. 1996, AJ, 112, 839
Croton, D. J., et al. 2006, MNRAS, 365, 11
de Koff, S., Baum, S. A., Sparks, W. B., Biretta, J., Golombek, D., Macchetto, F., McCarthy, P., & Miley, G. K. 1996, ApJS, 107, 621
de Koff, S., et al. 2000, ApJS, 129, 33
di Matteo, T., Springel, V., & Hernquist, L. 2005, Nature, 433, 604
Donzelli, C. J., Chiaberge, M., Macchetto, F. D., Madrid, J. P., Capetti, A., & Marchesini, D. 2007, ApJ, 667, 780
Dopita, M. A., Koratkar, A. P., Allen, M. G., Tsvetanov, Z. I., Ford, H. C., Bicknell, G. V., & Sutherland, R. S. 1997, ApJ, 490, 202
Faber, S. M., et al. 2007, ApJ, 665, 265
Fabian, A. C. 1999, MNRAS, 308, L39
Fanaroff, B. L., & Riley, J. M. 1974, MNRAS, 167, 31P
Ferrarese, L., & Merritt, D. 2000, ApJ, 539, L9
Floyd, D. J. E., et al. 2008, ApJS, 177, 148
Gebhardt, K., et al. 2000, ApJ, 539, L13
Gunn, J. E. 1979, in Active Galactic Nuclei, ed. C. Hazard & S. Mitton (Cambridge: Cambridge Univ. Press), 213
Habe, A., & Ikeuchi, S. 1985, ApJ, 289, 540
Haehnelt, M. G., & Rees, M. J. 1993, MNRAS, 263, 168
Holt, J., Tadhunter, C. N., González Delgado, R. M., Inskip, K. J., Rodriguez, J., Emonts, B. H. C., Morganti, R., & Wills, K. A. 2007, MNRAS, 381, 611
Holt, J., Tadhunter, C. N., & Morganti, R. 2009, MNRAS, 400, 589
Hopkins, P. F., Hernquist, L., Cox, T. J., Di Matteo, T., Robertson, B., & Springel, V. 2005, ApJ, 630, 716
Hopkins, P. F., Hernquist, L., Cox, T. J., Di Matteo, T., Robertson, B., & Springel, V. 2006, ApJS, 163, 1
Jones, T. W., Ryu, D., & Engel, A. 1999, ApJ, 512, 105
Kaiser, C. R., Schoenmakers, A. P., & Röttgering, H. J. A. 2000, MNRAS, 315, 381
Kauffmann, G., & Haehnelt, M. 2000, MNRAS, 311, 576
Khochfar, S., & Burkert, A. 2005, MNRAS, 359, 1379
Koekemoer, A. M., Fruchter, A. S., Hook, R. N., & Hack, W. 2002, in The 2002 HST Calibration Workshop: Hubble after the Installation of the ACS and the NICMOS Cooling System, ed. S. Arribas, A. Koekemoer, & B. Whitmore (Baltimore, MD: STScI), 337
Koekemoer, A. M., O'Dea, C. P., Sarazin, C. L., McNamara, B. R., Donahue, M., Voit, G. M., Baum, S. A., & Gallimore, J. F. 1999, ApJ, 525, 621
Kormendy, J., & Richstone, D. 1995, ARA&A, 33, 581
Lauer, T. R., et al. 2005, AJ, 129, 2138
Leitherer, C., et al. 1999, ApJS, 123, 3
Machalski, J., Kozieł-Wierzbowska, D., Jamrozy, M., & Saikia, D. J. 2008, ApJ, 679, 149

Maybhate, A., et al. 2010, ACS Instrument Handbook, version 9.0 (Baltimore, MD: STScI)
Mack, K.-H., Klein, U., O'Dea, C. P., & Willis, A. G. 1997, A&AS, 123, 423
Madrid, J. P., et al. 2006, ApJS, 164, 307
Magorrian, J., et al. 1998, AJ, 115, 2285
Martel, A. R., et al. 1999, ApJS, 122, 81
McCarthy, P. J. 1993, ARA&A, 31, 639
McCarthy, P. J., Miley, G. K., de Koff, S., Baum, S. A., Sparks, W. B., Golombek, D., Biretta, J., & Macchetto, F. 1997, ApJS, 112, 415
O'Dea, C. P., Koekemoer, A. M., Baum, S. A., Sparks, W. B., Martel, A. R., Allen, M. G., Macchetto, F. D., & Miley, G. K. 2001, AJ, 121, 1915
Osterbrock, D. E., & Ferland, G. J. 2006, Astrophysics of Gaseous Nebulae and Active Galactic Nuclei (2nd ed., Sausalito, CA: Univ. Science Books)
Parma, P., Murgia, M., Morganti, R., Capetti, A., de Ruiter, H. R., & Fanti, R. 1999, A&A, 344, 7
Pérez-González, P. G., et al. 2008, ApJ, 675, 234
Privon, G. C., O'Dea, C. P., Baum, S. A., Axon, D. J., Kharb, P., Buchanan, C. L., Sparks, W., & Chiaberge, M. 2008, ApJS, 175, 423
Quillen, A. C., & Bland-Hawthorn, J. 2008, MNRAS, 386, 2227
Rees, M. J. 1989, MNRAS, 239, 1P
Robinson, R. D., Cram, L. E., & Giampapa, M. S. 1990, ApJS, 74, 891
Salpeter, E. E. 1955, ApJ, 121, 161
Scannapieco, E., Silk, J., & Bouwens, R. 2005, ApJ, 635, L13
Schawinski, K., et al. 2006, Nature, 442, 888
Schilizzi, R. T., et al. 2001, A&A, 368, 398
Schmidt, M., Schneider, D. P., & Gunn, J. E. 1991, in ASP Conf. Ser. 21, The Space Distribution of Quasars, ed. D. Crampton (San Francisco, CA: ASP), 109
Schoenmakers, A. P., de Bruyn, A. G., Röttgering, H. J. A., & van der Laan, H. 2000a, MNRAS, 315, 395
Schoenmakers, A. P., de Bruyn, A. G., Röttgering, H. J. A., van der Laan, H., & Kaiser, C. R. 2000b, MNRAS, 315, 371
Silk, J., & Rees, M. J. 1998, A&A, 331, L1
Silverman, J. D., et al. 2008, ApJ, 675, 1025
Smith, E. P., & Heckman, T. M. 1989, ApJ, 341, 658
Sodroski, T. J., et al. 1994, ApJ, 428, 638
Spinrad, H., Marr, J., Aguilar, L., & Djorgovski, S. 1985, PASP, 97, 932
Springel, V., Di Matteo, T., & Hernquist, L. 2005, MNRAS, 361, 776
Tohline, J. E., Simonson, G. F., & Caldwell, N. 1982, ApJ, 252, 92
Tran, H. D., Tsvetanov, Z., Ford, H. C., Davies, J., Jaffe, W., van den Bosch, F. C., & Rest, A. 2001, AJ, 121, 2928
Tremblay, G. R., Chiaberge, M., Donzelli, C. J., Quillen, A. C., Capetti, A., Sparks, W. B., & Macchetto, F. D. 2007, ApJ, 666, 109
Tremblay, G. R., et al. 2009, ApJS, 183, 278
Tubbs, A. D. 1980, ApJ, 241, 969
Urry, C. M., & Padovani, P. 1995, PASP, 107, 803
Vázquez, G. A., & Leitherer, C. 2005, ApJ, 621, 695
Wuyts, S., et al. 2009, ApJ, 700, 799
York, D. G., et al. 2000, AJ, 120, 1579
Zirbel, E. L. 1997, ApJ, 476, 489